AIAA Aviation
August 12-14, 2013, Los Angeles, CA
2013 Aviation Technology, Integration, and Operations Conference

Spatio-Temporally Correlated Wind Uncertainty Model for Simulation of Terminal Airspace Operations

Monish D. Tandale*, V. V. S. Sai Vaddi†, Sydney Lin‡ and Prasenjit Sengupta§
Optimal Synthesis Inc., Los Altos, CA, 94022-2777

This paper deals with modeling the uncertainty associated with wind forecasts. National Oceanic and Atmosphere Administration's (NOAA's) RAPid Refresh (RAP) product is used as the wind forecast product. Actual aircraft measured data obtained by Aircraft Communications Addressing and Reporting System (ACARS) is treated as the 'actual' wind data. The paper creates a spatio-temporally correlated model for the error between the RAP and ACARS data. The error model is treated as the uncertainty in wind forecast. The wind uncertainty model captures the statistics of the North and East wind components as a function of altitude. It captures the correlation of errors both in the spatial and temporal domains. Furthermore, the paper develops an approach to generate sample random wind profiles for use in Monte Carlo simulations. The ability to generate random samples of wind facilitates evaluation of the robustness of NextGen concepts when subject to realistic wind uncertainties. The overall approach is illustrated for the terminal airspace of the San Francisco International Airport (SFO).

I. Introduction

Terminal airspaces the major airports in the National Airspace System (NAS) have been identified as areas of high traffic density and congestion. Consequently researchers in academia, industry and government have focused on analysis of terminal airspace operations to relieve system-wide congestions in the NAS. The following NextGen concepts[1-5] are being developed for terminal airspace super-density operations:

1. Automation for optimal scheduling, sequencing, route assignment and runway assignment based on optimization algorithms[6, 7]
2. 4D-trajectory management for scheduling conflict free trajectories using Area Navigation (RNAV) and Required Navigation Performance (RNP) routes[8, 9]
3. Conflict-free continuous descent arrivals from the top of descent to the runway threshold for multiple flights to multiple airports of a metroplex[10-12]
4. Ground based automation systems for conflict detection, separation assurance[13] and merging and spacing operations
5. Airborne merging and spacing technologies[14-18]
6. Very closely spaced parallel runway operations and simultaneous operations on intersecting runway under instrument meteorological conditions[8, 19]
7. Integrated arrival, departure[20, 21] and surface operations[22]
8. Optimal runway configuration management based on predicted weather and demand[23]

Successful implementation and realization of benefits from most of the above listed concepts and technologies require answers to the following questions:

1. What is the spatial uncertainty associated with an aircraft's predicted position at a given time in future?
2. What is the uncertainty associated with an aircraft's Time of Arrival (TOA) at a specified waypoint such as the meter fix or runway?
3. What is the accuracy (or uncertainty) with which an aircraft can maintain self-separation with respect to a leading aircraft?

* Senior Research Scientist, 95 First Street, monish@optisyn.com, Senior Member AIAA
† Senior Research Scientist, 95 First Street, vaddi@optisyn.com, Senior Member AIAA
‡ Research Engineer, 95 First Street, slin@optisyn.com
§ Research Scientist, 95 First Street, sengupta@optisyn.com, Senior Member AIAA

Wind prediction uncertainty is one of the primary uncertainties in terminal area operations and an understanding of this uncertainty is critical to answering the questions listed above.

Also, computer simulations are performed to evaluate NextGen concepts before their eventual deployment in operations. To achieve sufficient realism, the ambient wind field must be incorporated in the computer simulation. The predicted wind field is available from weather products such as Rapid Update Cycle (RUC)[24] or RAPid Refresh (RAP)[25]. However, the actual wind experienced by the aircraft does not match the predicted wind exactly. Truth wind fields must be generated for the simulation based on a wind prediction uncertainty model. Monte Carlo simulation is frequently used for stochastic analysis of terminal airspace operations. Given a predicted wind field, a random wind uncertainty profile must be created for each Monte Carlo iteration, to simulate the actual wind experienced in the simulation.

Realistic wind profiles are expected to exhibit spatio-temporal correlation, i.e. the wind should be similar at nearby locations and nearby times (even across different routes). Uncorrelated wind perturbations can cause unnatural artifacts such as: (i) a flight experiencing alternate head wind and tail wind at successive times or (ii) the trailing flight experiencing completely different wind from the leading aircraft.

This paper describes a methodology to

1. characterize the magnitude and spatio-temporal correlation of the uncertainty from recorded data and
2. generate spatio-temporally correlated wind uncertainty profiles for terminal airspace simulation.

The rest of the paper is organized as follows. Section II provides an overview of the approach. The sources of the predicted and observed wind data are described in Section III. Section IV describes the wind uncertainty modeling framework. Section V describes the multi-variate Gaussian model for wind uncertainty. Section VI describes the process of estimating the wind uncertainty parameters such as mean, variance and correlation coefficient from data. The procedure for generating spatio-temporally correlated random wind fields from the calibrated wind uncertainty model is presented in Section VII. Section VIII summarizes the wind uncertainty modeling process. The application of the uncertainty modeling process to the SFO terminal airspace is described in Section X. Finally, Section XI lists the salient features of the developed wind uncertainty model and unique contributions of this research effort.

II. Approach

In this work, the wind is modeled using two components: (i) North wind component (W_N), and (ii) East wind component (W_E). The two components can also be interpreted in terms of wind magnitude and wind heading. The wind components are modeled as functions of spatial coordinates: latitude (τ), longitude (λ), and altitude (h) and time (t).

$$W_N = W_N(\tau, \lambda, h, t) \qquad W_E = W_E(\tau, \lambda, h, t) \tag{1}$$

Each component of the wind is in turn modeled as the sum of a deterministic component (forecast) and a stochastic component (forecast error). The RAPid Refresh (RAP)[25] forecast provided by the National Oceanic and Atmospheric Administration (NOAA) is used as the deterministic component.

$$W_N = W_{N\_RAP}(\tau, \lambda, h, t) + \Delta W_N(\tau, \lambda, h, t) \tag{2}$$

$$W_E = W_{E\_RAP}(\tau, \lambda, h, t) + \Delta W_E(\tau, \lambda, h, t) \tag{3}$$

where W_{N_RAP} and W_{E_RAP} represent the RAP forecast components along the North and East directions respectively; and ΔW_N and ΔW_E represent the RAP forecast errors along the North and East directions respectively.

RAP provides the forecast at discrete points in both the horizontal and vertical planes. Interpolation schemes are used for intermediate spatial locations. The current approach also models the uncertainty components at discrete spatial locations. Figure 1 shows a sample discretization of the arrival routes in San Francisco (SFO) terminal airspace. Each discrete segment is referred to as a server and represented by s_i, for $i = 1..n$. Each server is expected to be characterized by horizontal position coordinates and an altitude. Note that this approach was originally developed for discrete time/space; however interpolation can be used to determine values for any continuous time/space simulation.

The wind uncertainty components are modeled as high-dimensional random vectors of size: $N_s = n \times N_t$, where N_t is the number of time units resulting from the discretization in the time domain. The number of servers is determined by the geographic area of interest. For terminal area operations, the geographic area of interest could be the entire TRACON or simply the arrival routes in the TRACON as shown in Figure 1. The total time horizon and the temporal discretization are dictated by the needs of the terminal airspace operation simulation. Current research adopted a 1-hour duration to match the duration of the RAP forecast. A temporal discretization of 1 minute is also used to match the terminal airspace simulation requirements. However, both these numbers can be arbitrarily picked to suit the needs of the simulation.

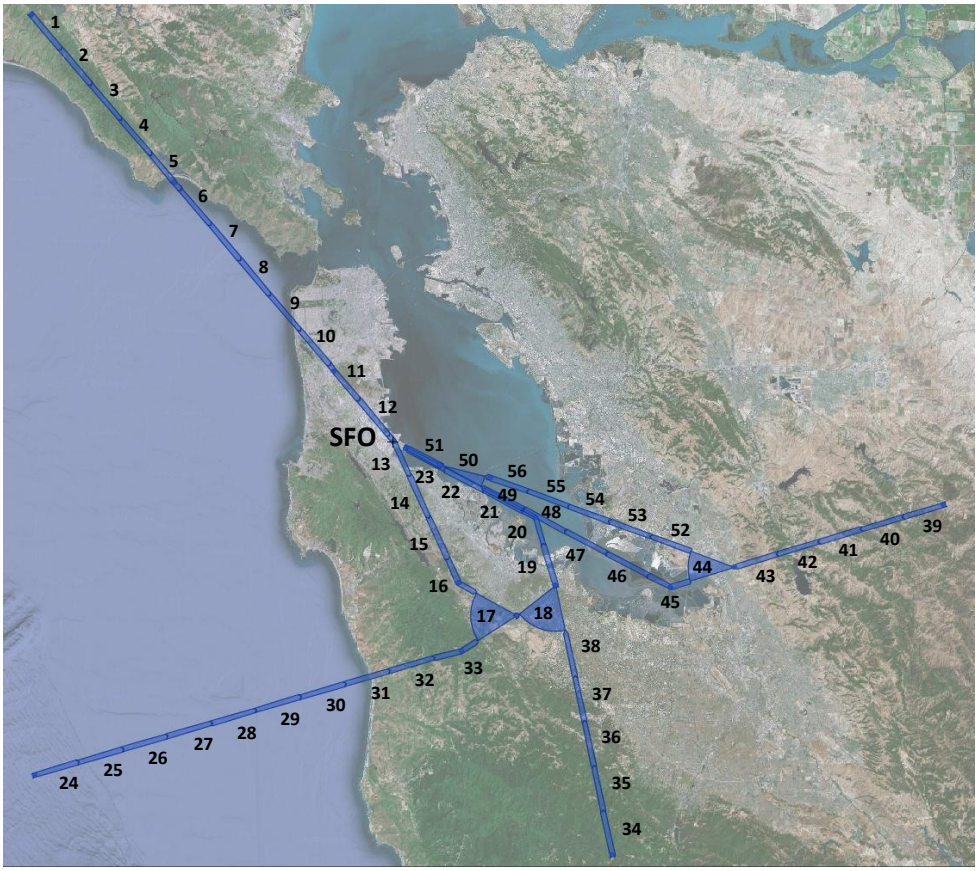

Figure 1. Discretized Terminal Airspace Routes at SFO

With the above discretization along space and time, the wind uncertainty components finally assume the form of a high-dimensional vector of length N_s as shown below:

$$\Delta W_{N\_vec} = \left[\Delta W_N(s_{1,1}), \Delta W_N(s_{1,2}), .. \Delta W_N(s_{1,60}), \Delta W_N(s_{2,1}), .. \Delta W_N(s_{n,1}), .. \Delta W_N(s_{n,60})\right] \quad (4)$$

$$\Delta W_{E\_vec} = \left[\Delta W_E(s_{1,1}), \Delta W_E(s_{1,2}), .. \Delta W_E(s_{1,60}), \Delta W_E(s_{2,1}) .. \Delta W_E(s_{n,1}), .. \Delta W_E(s_{n,60})\right] \quad (5)$$

where $s_{i,j}$ represents the i^{th} server at the j^{th} time-discretization. The component $\Delta W_N(s_{i,j})$ represents the North-wind uncertainty at the i^{th} server at the j^{th} time-discretization. ΔW_{N_vec} and ΔW_{E_vec} are vectors that represent the wind uncertainty components along the North and East directions respectively. These two vectors cover the entire spatial and temporal domains of interest.

Having represented the wind using a multi-dimensional vector, the objectives of this research can now be stated as follows:

1. Estimate and model realistic probability distributions $p_N(\Delta W_{N\_vec})$ and $p_E(\Delta W_{E\_vec})$ associated with the random vectors ΔW_{N_vec} and ΔW_{E_vec}.
2. Develop algorithmic framework to generate random samples from the probability distributions $p_N(\Delta W_{N\_vec})$ and $p_E(\Delta W_{E\_vec})$.

The following are the expectations from the wind-uncertainty models:

1. Realistic wind profiles are expected to exhibit spatial and temporal correlation, i.e. the wind should be similar at nearby locations and nearby times. Uncorrelated wind perturbations can cause unnatural artifacts such as: (i) a flight experiencing alternate head wind and tail wind at successive times, or (ii) a closely trailing flight experiencing a completely different wind than the leading aircraft.
2. The magnitude of the wind uncertainty is expected to depend on the altitude of the aircraft.

Section III describes the wind data sources used in modeling the probability distributions $p_N(\Delta W_{N\_vec})$ and $p_E(\Delta W_{E\_vec})$. Section IV describes the wind uncertainty modeling framework. Section VIII describes the random wind profile generation framework.

III. Wind Data Sources

The wind uncertainty is defined as the deviation between the actual wind and the predicted (forecasted) wind. Therefore, one way to model the probability distribution associated with the deviations is to study the statistical properties a large number of actual observed deviations. This requires the following data: (i) actual wind data and (ii) forecast wind data. In this research, actual wind measurements observed by aircraft flying in the NAS and reported through the Aircraft Communications Addressing and Reporting System (ACARS), are used as the actual data. As described earlier, the forecast is obtained from RAP.

A. ACARS Data

Many commercial aircraft operating today are equipped with sensors that can provide real-time weather observations (primarily winds and temperatures) via radio downlinks. The Meteorological Assimilation Data Ingest System's (MADIS)[26] automated aircraft dataset provides ACARS[27] data obtained from many U.S. airlines. Each participating aircraft provides the position and wind information $(\tau, \lambda, h, t, W_N, W_E)$ at approximately one-minute intervals. Since this data is obtained from actual aircraft flying through the airspace, the ACARS data is in general not available for any arbitrary location and time. It is only available for those spatial locations and times that the aircraft actually visited. Moreover, all aircraft do not necessarily report this data. However, a large amount of historical data is available to characterize the statistics of the wind uncertainty. Figure 2 shows sample trajectories of aircraft operating in the SFO terminal area that reported wind data using ACARS.

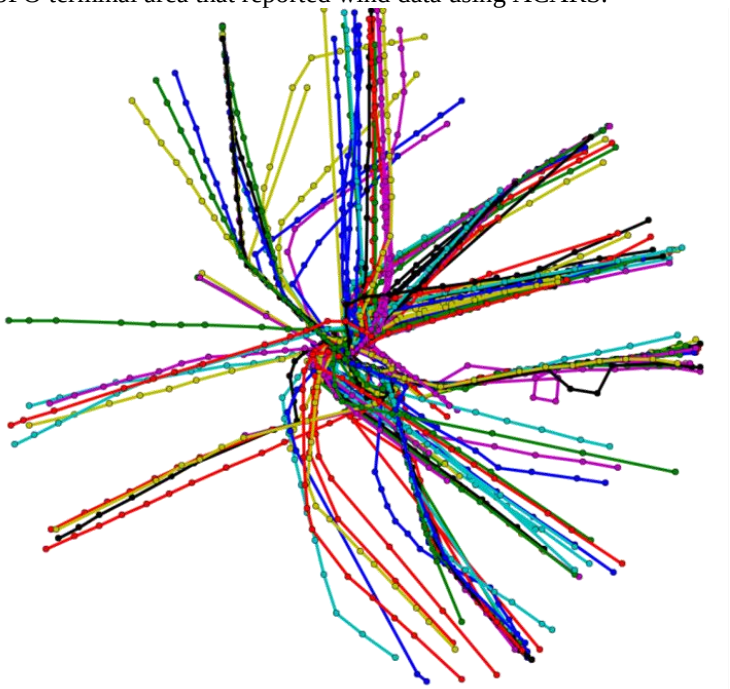

Figure 2. Sample Trajectories of ACARS Equipped Aircraft in the SFO Terminal Area

B. RAP Data

The National Oceanic and Atmosphere Administration (NOAA) provides wind and atmospheric predictions for the entire United States. As noted before, these forecasts can be obtained through a weather product referred to as RAPid Refresh[25]. RAP is an operational weather prediction system covering North America that updates on an hourly basis. It consists of a numerical forecast model and an analysis/assimilation system to initialize that model. RAP provides 1-18 hour forecasts, updated hourly using a 13-km horizontal resolution and 50 vertical levels. It provides the predicted North and East components of the wind. Unlike the ACARS data, RAP data is available over a much larger grid of spatial locations. In this work, a bilinear interpolation scheme has been implemented to compute the wind predictions for spatial locations that do not exactly match the grid points.

Although the current work focuses on wind modeling, it should be noted that the approach is applicable to other atmospheric data such as temperature and pressure. In that context, it is worth noting that both ACARS and RAP provide temperature and pressure data as well.

IV. Wind Uncertainty Modeling Framework

A data-based approach is used for modeling the wind uncertainty in this research. Figure 3 illustrates the overall framework.

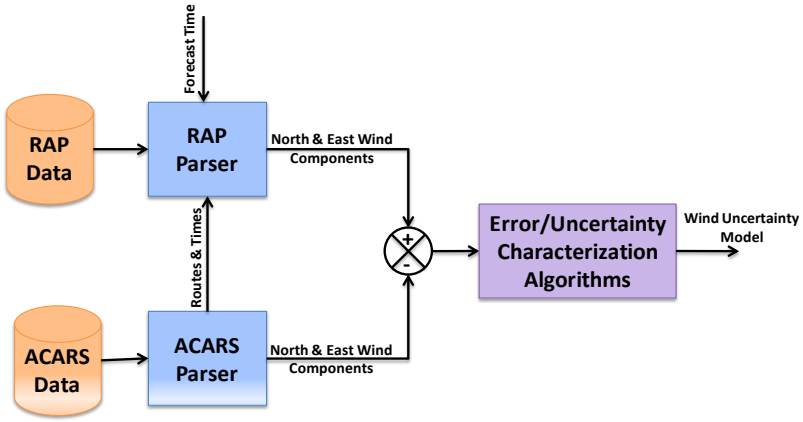

Figure 3. Block Diagram of the Wind Uncertainty Characterization Framework

The first step in this process is to collect and analyze past RAP and ACARS data. The recorded locations ACARS data are a subset of the predicted locations of RAP. Therefore, the wind prediction errors are computed for only those locations and times at which the ACARS data was recorded. The RAP predicted wind at the ACARS observation points can be obtained by appropriately interpolating the RAP data. Figure 4 shows a comparison between the ACARS wind data recorded by an aircraft flying along the GOLDN6 arrival into SFO and the RAP wind predictions for the same.

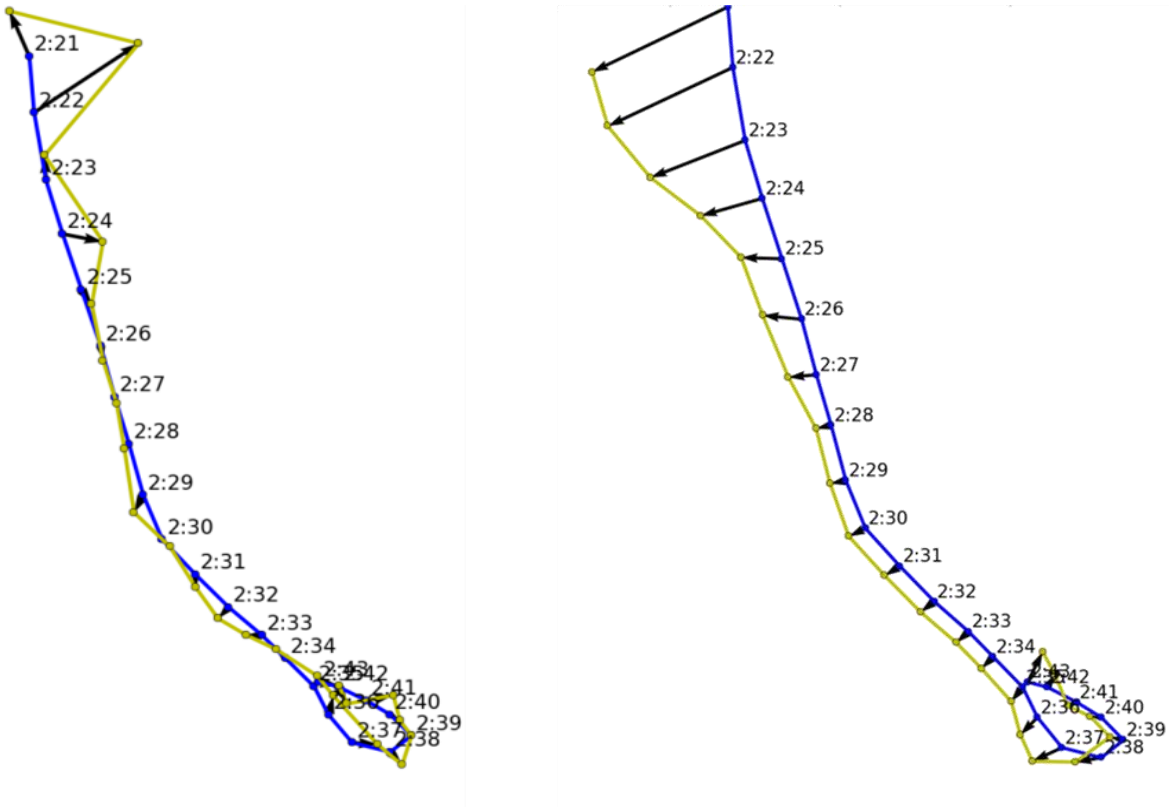

ACARS Data (Actual Recorded Winds) **RAP Data (1-hr Wind Prediction)**

Figure 4. Comparison between MADIS Recorded Winds and RAP Wind Predictions for the GOLDN6 Arrival into SFO

The length of the arrow indicates the magnitude of the wind and the direction of the arrow indicates the heading of the wind. Clearly, the actual is different from the predicted wind. It is also clear from these plots that the deviation is not simply random at all locations. The wind errors are correlated along the path that the aircraft traveled. This research modeled the correlated behavior using a multi-variate probability distribution which is discussed in the following section.

V. Multi-Variate Gaussian Model for Wind Uncertainty

The wind prediction error can be thus calculated as:

$$\Delta W_N = W_{N\_ACARS} - W_{N\_RAP} \quad (6)$$

$$\Delta W_E = W_{E\_ACARS} - W_{E\_RAP} \quad (7)$$

where W_{N_ACARS} and W_{E_ACARS} denote the North and East components of the wind obtained from ACARS; and W_{N_RAP} and W_{E_RAP} denote the North and East components of the wind obtained from RAP for the same spatial and temporal location as the ACARS data.

A simplistic model of uncertainty would simply involve generating the random numbers for each component of the wind uncertainty vectors independently of the other components. The various components of the wind uncertainty vectors are the values at different spatial locations at different times. An obvious deficiency of this approach is that it does not capture and spatial and temporal correlations of the prediction errors.

This research jointly generates all the components of the random wind uncertainty vectors to enforce spatio-temporal correlation. Figure 1 enumerates the North and East components of the wind uncertainty vector.

t_1				t_2					t_m			
s_1	s_2	...	s_n	s_1	s_2	...	s_n	...	s_1	s_2	...	s_n
ΔW_N^{11}	ΔW_N^{21}	...	ΔW_N^{n1}	ΔW_N^{12}	ΔW_N^{22}	...	ΔW_N^{n2}	...	ΔW_N^{1m}	ΔW_N^{2m}	...	ΔW_N^{nm}
ΔW_E^{11}	ΔW_E^{21}	...	ΔW_E^{n1}	ΔW_E^{12}	ΔW_E^{22}	...	ΔW_E^{n2}	...	ΔW_E^{1m}	ΔW_E^{2m}	...	ΔW_E^{nm}

Figure 5. North and East Wind Uncertainty Vectors

This approach involves modeling the wind uncertainty components along North and East directions as independent multi-variate Gaussian distributions:

$$\Delta W_N \sim N(\mu_N, \Sigma_N) \quad (8)$$

$$\Delta W_E \sim N(\mu_E, \Sigma_E) \quad (9)$$

where μ_N and μ_E represent the mean of the wind uncertainty vectors (of length N_s) associated with the North and East directions respectively; and Σ_N and Σ_E represent the covariance matrices (size $N_s \times N_s$) associated with the wind uncertainty along North and East directions respectively. Note that $N_s = n \times N_t$, where n is the number of servers and N_t is the discretization in the time domain.

Using the definition of the correlation coefficient $\rho_{x,y} = cov(X,Y)/\sigma_x\sigma_y$, each component of the covariance matrix can be written as

$$cov(X,Y) = \rho_{x,y}\sigma_x\sigma_y \quad (10)$$

Figure 6 shows the structure of the proposed covariance matrix for an example with $n = 3$ servers and $N_t = 3$ time discretizations, giving rise to a wind uncertainty random vector of size 9. Thus, the size of matrix is 9×9. Note that the 3×3 sub matrix shown in green in the top left corner denotes the covariance matrix for all the servers at the same time t_1. The orange squares illustrate the various covariance terms associated with the first server s_1 at all possible times. The diagonal terms outlined in black denote the variance associated with a server at a given time.

The multi-variate Gaussian representation of wind-uncertainty has the following features:

1. It accommodates spatial correlation in wind uncertainty. Therefore, wind samples generated using this model will result in nearby servers at the same time having similar wind components.
2. It accommodates temporal correlation of wind uncertainty. Therefore, wind samples at a given spatial location and nearby time instances will have similar wind components.

Figure 6. Structure of the Covariance Matrix

VI. Estimating the Wind Uncertainty from Actual Data

Having established the representation of the covariance matrix, the next step is to estimate the mean vectors μ_N, μ_E and the covariance matrices Σ_N, Σ_E using actual data. Since the covariance matrix is parameterized in terms of σ and ρ, estimating the mean and variance involves identifying parameters μ, σ, ρ from observed wind uncertainty data.

It is assumed that the following data is available:

1. A large number of ACARS North and East wind data samples each tagged by time, latitude, longitude, and altitude.
2. North and East wind components from RAP forecast data for the same time, latitude, longitude, and altitude of the ACARS data samples.

The above data can be used to determine the North and East component of the wind forecast errors for each of the ACARS data samples. However, it is unrealistic to expect to have actual wind data measurements at all the

servers (lat, lon, alt) at all times (t). Hence this research effort proposes an approach that is particularly amenable for computation using sparse wind error data. The approach is described in detail in the following sub sections.

A. Calculating the Mean (μ) and Variance (σ) of the Wind Errors

Ideally, given large amounts of data, the mean μ and variance σ of the wind errors can be determined as a function of the latitude, longitude, altitude and time.

$$\mu_{(server,t)} = \mu(lat, lon, alt, t) \qquad \sigma_{(server,t)} = \sigma(lat, lon, alt, t) \tag{11}$$

Since RAP provides a constant forecast for a 1-hour duration, there is no reason why the wind errors would be an explicit function of time. Hence we can drop the time dependency. Also, the wind errors are independent of the location in the horizontal plane (lat, lon), but vary with the altitude (alt). Hence, the mean and standard deviation are modeled as functions of altitude only.

$$\mu_{(server,t)} = \mu(alt) \qquad \sigma_{(server,t)} = \sigma(alt) \tag{12}$$

These mean and variance terms can be computed by simply binning all the observed forecast errors into different altitude levels and calculating the values for each bin. Figure 7 shows the relationship between wind uncertainty and altitude computed using 15 days of ACARS and RAP data around SFO. The box plot clearly portrays the high uncertainty and higher altitude. However, it should also be noted that magnitude of the nominal wind magnitude is also higher at higher altitudes. Also, note that the mean error is close to zero, but not exactly zero.

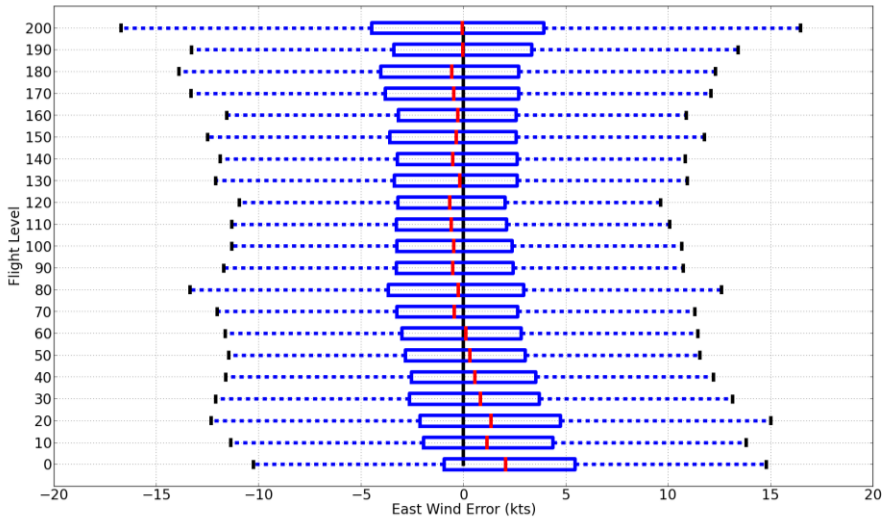

Figure 7. Wind Uncertainty as a Function of the Altitude

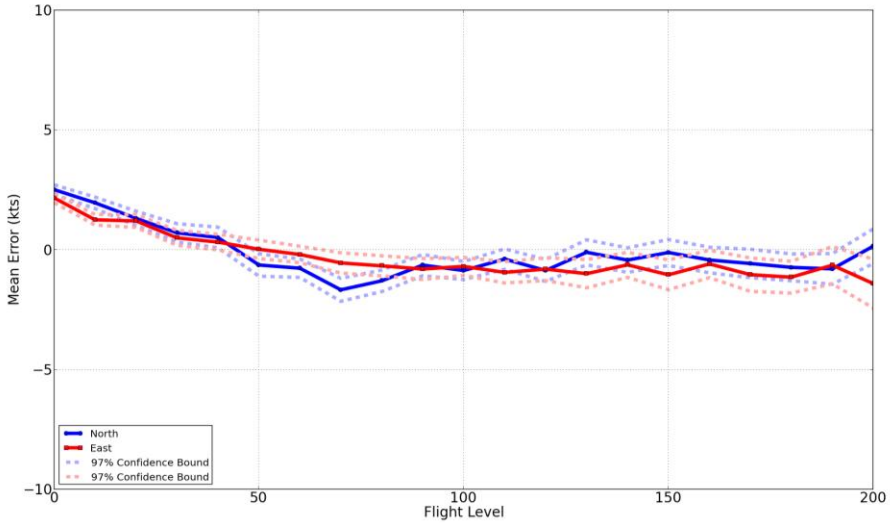

Figure 8. Mean of the North and East Wind Uncertainty as a Function of Altitude

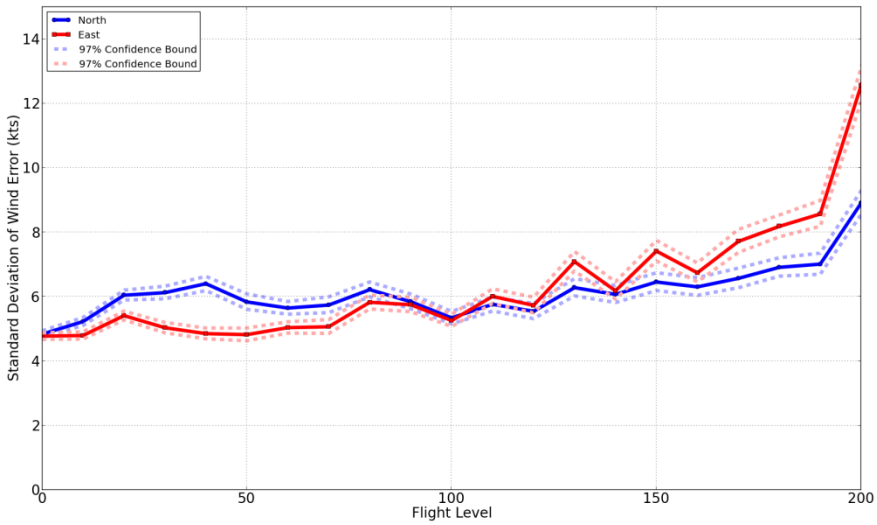

Figure 9. Standard Deviation of the North and East Wind Uncertainty as a Function of Altitude

Figure 8 and Figure 9 provide the mean and standard deviation respectively of the North and East components of the wind uncertainty. The increase in wind prediction uncertainty with altitude can be seen from Figure 8. The 97% confidence bounds on the calculated mean and standard deviation values are shown as dashed lines in both figures, and serve as indicators of the quality of the results. This is because statistics such as mean and standard deviation are calculated from *samples*, and are therefore generally different from the unknown statistics of the *population*. In this work, calculation of confidence bounds is essential because the number of samples can greatly vary with respect to altitude. For instance, when building wind error models in the terminal area, fewer wind measurements are obtained at cruise altitudes than at flight levels lower than 20,000 ft.

B. Calculating the Correlation Coefficients (ρ) for the Wind Errors

Consider the two correlation terms ρ_{12} and ρ_{45} from Figure 6. The term ρ_{12} denotes the correlation between server s_1 and server s_2 at the same time t_1. The term ρ_{45} denotes the correlation between server s_1 and server s_2 at the same time t_2. The correlation between servers s_1 and s_2 at the same time instant should be the same irrespective of whether the absolute time is t_1 or t_2. Thus the correlation is dependent on the relative distance between the servers and relative time difference between the time instants of interest, and not the absolute values of location or time. Hence, the current work models the correlation ρ in the wind prediction uncertainty as a function of the relative distance δd between the two servers and the relative time δt between the two time instants of interest. The correlation between the i^{th} server at the k^{th} time instant and j^{th} server at the l^{th} time instant can be expressed as

$$\rho = f(\delta d_{ij}, \delta t_{lk}) \tag{13}$$

To derive this functional dependence, pairs of ACARS-RAP data samples are binned according to their spatial separation (relative distance) and temporal separation (relative time). The temporal separation resolution is chosen as 1 minute and the range is chosen as 0-30 minutes. The resolution of spatial separation is chosen as 1 nmi and the range is set to 60 nmi. Figure 10 shows the different bins and their correlation coefficients as a function of relative distance and relative time.

		Relative Time					
		0	1	2	3	4	..
Relative Distance	0	ρ_{00}	ρ_{01}	ρ_{02}	ρ_{03}	ρ_{04}	..
	1	ρ_{10}	ρ_{11}	ρ_{12}	ρ_{13}	ρ_{14}	..
	2	ρ_{20}	ρ_{21}	ρ_{22}	ρ_{23}	ρ_{24}	..
	3	ρ_{30}	ρ_{31}	ρ_{32}	ρ_{33}	ρ_{34}	..
	4	ρ_{40}	ρ_{41}	ρ_{42}	ρ_{43}	ρ_{44}	..
	:	:	:	:	:	:	⋱

Figure 10. Correlation Coefficient as a Function of Relative Time and Relative Distance

Consider a single bin in the above figure and let the number of data pairs in the bin be m. It should be noted that bins with very small spatial separation and very small temporal separation will not have any data pairs as it would violate the inter-aircraft separation requirements. Let the two data samples within a pair be represented by the symbols a and b. Consider the following matrix representation of the North component errors for all the pairs in a given bin

$$\begin{bmatrix} (\Delta W_N)_{a1} & (\Delta W_N)_{b1} \\ (\Delta W_N)_{a2} & (\Delta W_N)_{b2} \\ (\Delta W_N)_{a3} & (\Delta W_N)_{b3} \\ \vdots & \vdots \\ (\Delta W_N)_{a(m-1)} & (\Delta W_N)_{b(m-1)} \\ (\Delta W_N)_{am} & (\Delta W_N)_{bm} \end{bmatrix} \tag{14}$$

where the subscript ai and bi refer to the first and the second element in the i^{th} data pair. The covariance matrix for the above data can in turn be expressed as the following 2×2 matrix:

$$\begin{bmatrix} C_{aa} & C_{ab} \\ C_{ab} & C_{bb} \end{bmatrix} \tag{15}$$

The correlation coefficient for the bin which is in turn is characterized by a spatial separation and temporal separation can now be calculated as follows:

$$\rho = \frac{C_{ab}}{\sqrt{C_{aa}}\sqrt{C_{bb}}} \tag{16}$$

The procedure described above is repeated for all the $(60 \times 30 = 1800)$ bins. The correlation coefficients thus obtained using 15 days ACARS and RAP data around SFO is shown in Figure 11. As expected, the spatial correlation is strong for smaller spatial separations; it gradually wanes as the relative distance increases. The data shows that the correlation remains constant over time.

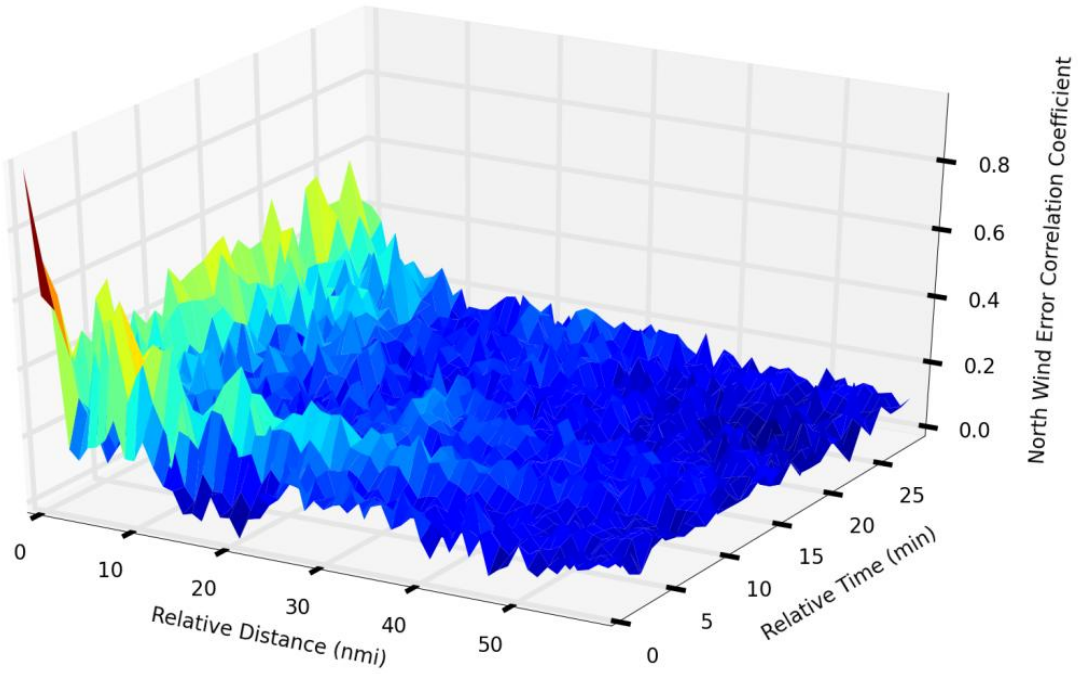

Figure 11. Correlation Coefficient as a Function of Relative Distance and Relative Time

Function fits and interpolation are used to determine the correlation coefficient at any arbitrary relative time and relative distance. Also note that the data provided no correlation between the North and East components of the wind, as expected.

VII. Constructing the Covariance Matrix from the Estimated Mean μ, Variance σ and Correlation Coefficient ρ

The covariance matrix can be assembled from the estimated mean μ, variance σ and correlation coefficient ρ as follows The covariance term between the i^{th} server at the k^{th} time instant and j^{th} server at the l^{th} time instant is modeled as follows: $\Sigma_{ij} = \rho_{|i-j||l-k|}\sigma_i\sigma_j$.

		t_1			t_2			t_3		
		s_1	s_2	s_3	s_1	s_2	s_3	s_1	s_2	s_3
t_1	s_1	σ_1^2	$\rho_{10}\sigma_1\sigma_2$	$\rho_{20}\sigma_1\sigma_3$	$\rho_{01}\sigma_1^2$	$\rho_{11}\sigma_1\sigma_2$	$\rho_{21}\sigma_1\sigma_3$	$\rho_{02}\sigma_1^2$	$\rho_{12}\sigma_1\sigma_2$	$\rho_{22}\sigma_1\sigma_3$
	s_2	$\rho_{10}\sigma_1\sigma_2$	σ_2^2	$\rho_{10}\sigma_2\sigma_3$	$\rho_{11}\sigma_1\sigma_2$	$\rho_{01}\sigma_2^2$	$\rho_{11}\sigma_2\sigma_3$	$\rho_{12}\sigma_1\sigma_2$	$\rho_{02}\sigma_2^2$	$\rho_{12}\sigma_2\sigma_3$
	s_3	$\rho_{20}\sigma_1\sigma_3$	$\rho_{10}\sigma_2\sigma_3$	σ_3^2	$\rho_{21}\sigma_1\sigma_3$	$\rho_{11}\sigma_2\sigma_3$	$\rho_{01}\sigma_3^2$	$\rho_{22}\sigma_1\sigma_3$	$\rho_{12}\sigma_2\sigma_3$	$\rho_{02}\sigma_3^2$
t_2	s_1	$\rho_{01}\sigma_1^2$	$\rho_{11}\sigma_1\sigma_2$	$\rho_{21}\sigma_1\sigma_3$	σ_1^2	$\rho_{10}\sigma_1\sigma_2$	$\rho_{20}\sigma_1\sigma_3$	$\rho_{01}\sigma_1^2$	$\rho_{11}\sigma_1\sigma_2$	$\rho_{21}\sigma_1\sigma_3$
	s_2	$\rho_{11}\sigma_1\sigma_2$	$\rho_{01}\sigma_2^2$	$\rho_{11}\sigma_2\sigma_3$	$\rho_{10}\sigma_1\sigma_2$	σ_2^2	$\rho_{10}\sigma_2\sigma_3$	$\rho_{11}\sigma_1\sigma_2$	$\rho_{01}\sigma_2^2$	$\rho_{11}\sigma_2\sigma_3$
	s_3	$\rho_{21}\sigma_1\sigma_3$	$\rho_{11}\sigma_2\sigma_3$	$\rho_{01}\sigma_3^2$	$\rho_{20}\sigma_1\sigma_3$	$\rho_{10}\sigma_2\sigma_3$	σ_3^2	$\rho_{21}\sigma_1\sigma_3$	$\rho_{11}\sigma_2\sigma_3$	$\rho_{01}\sigma_3^2$
t_3	s_1	$\rho_{02}\sigma_1^2$	$\rho_{12}\sigma_1\sigma_2$	$\rho_{22}\sigma_1\sigma_3$	$\rho_{01}\sigma_1^2$	$\rho_{11}\sigma_1\sigma_2$	$\rho_{21}\sigma_1\sigma_3$	σ_1^2	$\rho_{10}\sigma_1\sigma_2$	$\rho_{20}\sigma_1\sigma_3$
	s_2	$\rho_{12}\sigma_1\sigma_2$	$\rho_{02}\sigma_2^2$	$\rho_{12}\sigma_2\sigma_3$	$\rho_{11}\sigma_1\sigma_2$	$\rho_{01}\sigma_2^2$	$\rho_{11}\sigma_2\sigma_3$	$\rho_{10}\sigma_1\sigma_2$	σ_2^2	$\rho_{10}\sigma_2\sigma_3$
	s_3	$\rho_{22}\sigma_1\sigma_3$	$\rho_{12}\sigma_2\sigma_3$	$\rho_{02}\sigma_3^2$	$\rho_{21}\sigma_1\sigma_3$	$\rho_{11}\sigma_2\sigma_3$	$\rho_{01}\sigma_3^2$	$\rho_{20}\sigma_1\sigma_3$	$\rho_{10}\sigma_2\sigma_3$	σ_3^2

Figure 12.Constructing the Covariance Matrix Using the Relative Correlation Terms

A key step in using the above covariance matrix for generating correlated random numbers is that the covariance matrix is positive definite so that Cholesky decomposition ($\Sigma = LL^T$) can be performed. The covariance matrix estimated using the above approach may not be positive definite due to the following reasons:

1. Numerical error in processing the data
2. Use of limited number of data samples
3. Sensor error in the MADIS wind observations

If the numerically generated covariance matrix is not positive definite, the nearest positive definite matrix can be constructed using the procedure described below. First, an Eigenvalue Decomposition is performed on the covariance matrix Σ such that:

$$\Sigma = VEV^T \tag{17}$$

where V is a square $(N_s \times N_s)$ matrix whose i^{th} column is the i^{th} eigenvector of Σ and E is a diagonal matrix whose diagonal elements are the eigenvalues of Σ. Note that symmetric matrices are diagonalizable and can always be decomposed into this form. Note that the covariance matrix Σ developed above is symmetric.

The second step involves finding the nearest positive definite matrix $\tilde{E}$ to the diagonal eigenvalue matrix E. Positive definite matrices have all positive eigenvalues. $\tilde{E}$ is a diagonal matrix which is computed by replacing the negative eigenvalues of the E matrix with zero as follows:

$$\begin{gathered} if\ E_{ii} > 0\ then\ \tilde{E}_{ii} = E_{ii} \\ Else \\ \tilde{E}_{ii} = 0 \end{gathered} \tag{18}$$

The approximated covariance matrix $\tilde{\Sigma}$ can be written as follows:

$$\tilde{\Sigma} = V\tilde{E}V^T \tag{19}$$

The approximation error introduced due to the replacement of the negative eigenvalues can be quantified by the relative change in the Frobenius norm of the covariance matrix.

$$\Sigma_{err} = \frac{\left|\Sigma - \tilde{\Sigma}\right|_{frobenius}}{|\Sigma|_{frobenius}} \tag{20}$$

The validity of the approximation requires that Σ_{err} be very small. Calculating all eigenvalues for the covariance matrix can be slow especially if the number of servers or the number of time instances is high. Hence, by using the Arnoldi algorithm[28] only the first few eigenvalues with the largest magnitudes and their corresponding eigenvectors can be chosen to construct the covariance matrix.

VIII. Random Wind Sample Generation Framework

The previous section described the procedure for estimating the μ_N, μ_E, Σ_N, and Σ_E corresponding to the multi-variate Gaussian distribution associated with the wind uncertainty. The current section deals with process for generating random wind samples from these distributions. Whereas generating uncorrelated random numbers is straight forward, the approach for generating correlated random numbers involves the following steps:

1. Factor the covariance matrix as follows $\Sigma = LL^T$. Note that the eigenvalue decomposition performed in Section VII can be used to determine the L matrix as follows:
$$L = V\sqrt{\tilde{E}} \tag{21}$$
where the square-root of $\tilde{E}$ is another diagonal matrix with entries $\sqrt{\tilde{E}_{ii}}$.
2. Generate a random vector η (length N_s) from an uncorrelated Gaussian distribution with zero mean and unit standard deviation.
3. Transform the uncorrelated random vector η: $(\eta_c = \mu + L\eta)$. It can be shown that $\eta_c \sim N(\mu, \Sigma)$.
4. The above process needs to be repeated both along the North and East directions.

IX. Summary of the Wind Uncertainty Modeling Process

The procedure for the wind uncertainty characterization and random wind profile generation can be summarized as follows:

1. Determine the MADIS wind observations in the given geographic area and time interval under consideration.
2. Obtain the RAP wind predictions for the same location and time instants as the MADIS wind observations.
3. Determine the wind prediction error by taking the difference between the MADIS and RAP data at the same location and time.
4. Classify the wind prediction error samples into bins for various altitude levels and determine the mean μ and variance σ of the wind prediction uncertainty as a function of the altitude.
5. Classify the wind prediction error sample pairs into bins for relative distance δd and relative time δt and determine the correlation coefficient ρ as a function of the relative distance and relative time.
6. Determine an appropriate function fit for the correlation coefficient as a function of relative distance and relative time.
7. Determine the spatial and temporal resolution of the grid for generating the random wind profiles.
8. Create the covariance matrix Σ for the random wind uncertainty vector using the mean and variance σ as a function of the altitude and the correlation coefficient $\rho(\delta d, \delta t)$.

9. Perform eigenvalue decomposition to ensure positive definiteness of the covariance matrix Σ and determine L such that $\Sigma = LL^T$.
10. Generate correlated random wind field by applying the transformation as $(\eta_c = \mu + L\eta)$ to an uncorrelated random vector $\eta \sim N(0,1)$.

X. Results

The approach described in the previous sections was applied to the SFO terminal airspace. Figure 1 shows the terminal area routes used in this example. The routes are discretized into 3 nmi servers which results in about 50 servers. The temporal domain is discretized into 1 minute intervals over a total of 60 minutes. The resulting wind uncertainty vectors are of length 2000 both along the North and East directions. ACARS and RAP data over a fifteen-day duration were used computing the μ_E, μ_N vectors and the covariance matrices Σ_E and Σ_N. The covariance matrices are approximated to the nearest positive definite versions using the procedure described in Section VII. The percentage change in the Frobenius norm was 0.65% indicating that the approximation error was very small. Even if only the largest 20 eigenvalues were used, the percentage error in the Frobenius norm was 5.26%. Wind uncertainty profiles were generated for the 50 servers at the 60 time instants using the framework described in Section VIII.

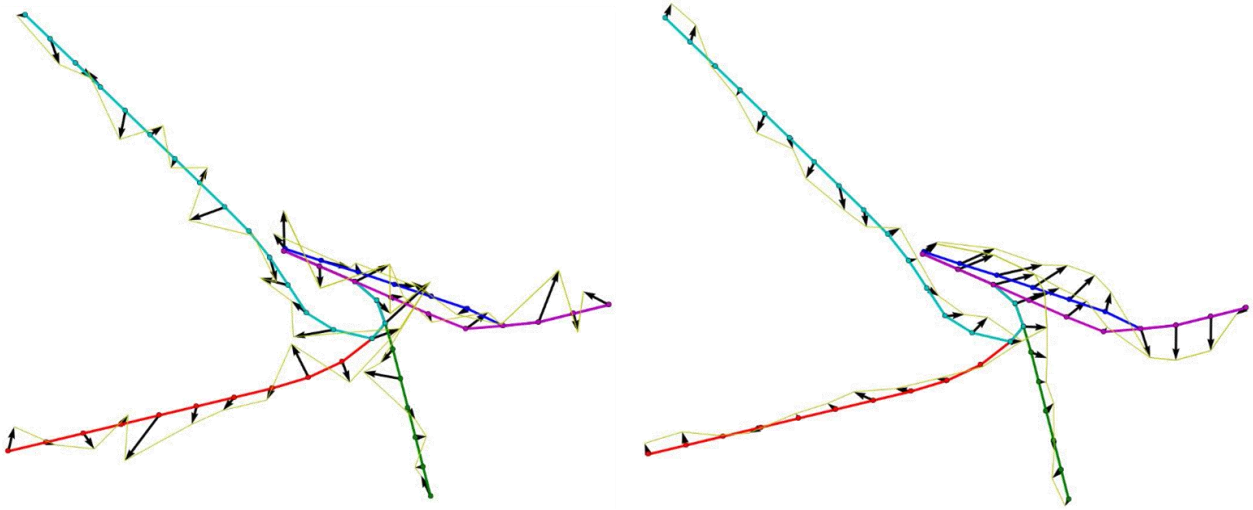

(a) Uncorrelated Wind Profile **(b) Spatially Correlated Wind Profile**

Figure 13. Correlated and Uncorrelated Wind Profiles along SFO Arrival Routes

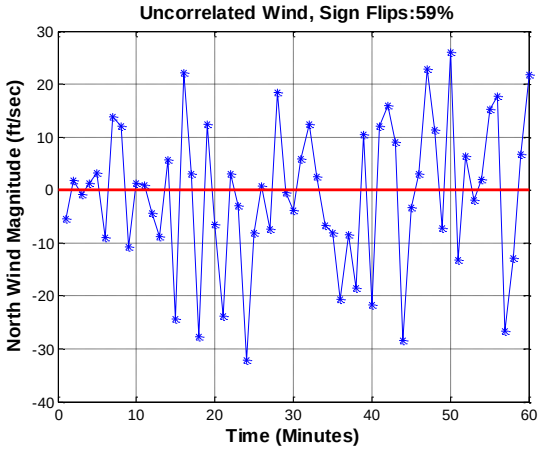

Figure 14. Temporal Behavior of Uncorrelated Wind Samples

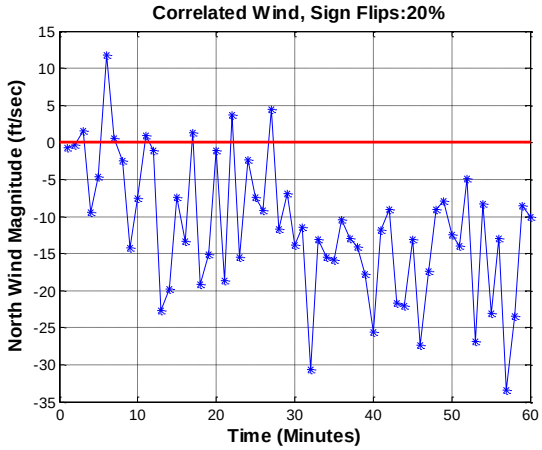

Figure 15. Temporal Behavior of Correlated Wind Samples

Figure 13 compares the correlated wind profiles generated using current research with the uncorrelated ones. The uncorrelated wind profile is shown in sub-figure (a) and the correlated wind profile is shown in sub-figure (b). The black arrows represent the wind magnitude and directions at the spatial locations (servers) indicated by solid circles at one particular time snap shot. It can be inferred from the sub-figure (a) that the wind magnitude and direction

change abruptly over nearby locations, indicating the absence of spatial correlation. On the hand the wind profile in sub-figure (a) consists of much smoother variation of the wind over the spatial domain. Thus continuous motion in the spatial domain results in continuous correlated variation of the wind.

Figure 13 illustrated the spatial correlation of the wind samples generating using the current approach. Figure 14 and Figure 15 illustrate the temporal correlation of the wind samples. The figures plot the North wind magnitude at a particular spatial location as a function of time. The uncorrelated wind sample shown in Figure 14 indicates high-frequency behavior characterized by the sign flips of the North wind component which is 59%. On the other hand the correlated wind sample in Figure 15 indicates that the sign flips are far fewer at 20%.

XI. Salient Features and Unique Contributions of Research

This paper presented a wind uncertainty modeling approach that calibrates the magnitude and spatio-temporal correlation based on RAP predictions and ACARS observations, and generates spatio-temporally correlated wind fields for terminal airspace simulations. The salient features of the wind uncertainty model developed under this research effort are as follows:

1. It models spatio-temporal correlation of wind errors along the same route and across different routes.
2. It captures the wind prediction uncertainty as a function of altitude.
3. The model structure is generic enough to accommodate any functional form of the spatio-temporal correlation.
4. The parameters of the model are derived from actual RAP and ACARS data.
5. The approach is generic, so it can be used for any airspace in the NAS.

The unique contributions of this work with respect to previously published literature on wind prediction uncertainty are as follows:

1. Ren and Clarke[29]: Ren and Clarke developed a wind uncertainty model suitable for consecutive flights pairs conducting continuous descent approaches while following the same ground tracks and vertical profiles. As such, their model is valid for a pair of consecutive flights flying along a single route. In contrast, the current model is applicable over a larger spatial and temporal domains.
2. Cole et al.[30]: This paper performed a detailed statistical characterization for both spatial and temporal correlation coefficient of the wind prediction uncertainty. However this paper does not provide a method to generate correlated random wind profiles for a terminal area routing structure.

Acknowledgments

This research was supported under NASA Phase II SBIR Contract No. NNX11CA08C monitored out of the NASA Ames Research Center. The authors would like to thank the COTR Mr. Douglas Isaacson and Technical Monitor Dr. Alexander Sadovsky both from NASA Ames Research Center. A special word of gratitude goes to Mr. John Robinson for his constant inputs, support, and encouragement of this research.

References

[1]"Concept of Operations for the Next Generation Air Transportation System, Version 3.2," Joint Planning and Development Office, September 30, 2010.

[2]Isaacson, D. R., Swenson, H. N., and Robinson III, J. E., "A Concept for Robust, High Density Terminal Air Traffic Operations," 10th AIAA Aviation Technology, Integration, and Operations Conference (ATIO), Fort Worth, TX, Sep. 13-15, 2010.

[3]"NextGen Avionics Roadmap, Version 1.0," Joint Planning and Development Office, October 24, 2008.

[4]Cheng V. H. L., Sweriduk G., Vaddi, S., Tandale M. D., Seo A., Abramson P., Koenke E., "Modeling Requirements to Support Assessment of NextGen Mid-Term Performance," AIAA-2009-6976, AIAA Aviation Technology, Integration, and Operations Conference, Hilton Head, SC, September 21 –23, 2009.

[5]Kopardekar, P., "NASA NextGen-Airspace Project", Presentation made at the NASA Airspace Systems Program Technical Interchange Meeting, Oct 2009, San Antonio, TX.

[6]Atkins, S., Capozzi B., and Choi, S., "Towards Optimal Route Assignment and Scheduling of Metroplex Traffic", Presentation made at the NASA Airspace Systems Program Technical Interchange Meeting, Oct 2009, San Antonio, TX.

[7]Capozzi B., Atkins, S. C., and Choi, S., "Towards Optimal Route Assignment and Scheduling of Metroplex Traffic", Proceedings of 9th AIAA Aviation Technology, Integration, and Operations Conference (ATIO), September 2009, Hilton Head, South Carolina.

[8]C. Devlin, M. Mills, R. Ottobre, S. Porter, and K. Sprong, "Applications and Benefits of RNP Approaches in the United States National Airspace System," AIAA-2005-7385, AIAA 5th ATIO and 16th Lighter-Than-Air Sys Tech. and Balloon Systems Conferences, Arlington, Virginia, Sep. 26-28, 2005.

[9]Smith, E. C., "A Study of Issuing Area Navigation (RNAV) Routing Changes in Terminal Airspace", *Proceedings of the 26th International Congress on Aeronautical Sciences*, Sep 2008, Anchorage, Alaska.

[10]Coppenbarger, R., Lanier, R., Sweet, D., and Dorsky, S., "Design and Development of the En Route Descent Advisor for Conflict-Free Arrival Metering," *Proceedings of AIAA Guidance, Navigation, and Control Conference*, Providence, Rhode Island, 2004

[11]Coppenbarger, R., Dyer, G., Hayashi, M., Lanier, R., Stell, L., and Sweet D., "Development and Testing of Automation for Efficient Arrivals in Constrained Airspace," Proceedings of the 27th International Congress of the Aeronautical Sciences, Nice, France, 2010.

[12]Coppenbarger, R., "Design, Development, and Testing of En Route Descent Advisor", Presentation made at the NASA Airspace Systems Program Technical Interchange Meeting, Oct 2009, San Antonio, TX.

[13]Tang, H., Robinson, J., Resiman, R., and Denery, D., "Tactical Conflict Detection in Terminal Airspace", Presentation made at the NASA Airspace Systems Program Technical Interchange Meeting, Oct 2009, San Antonio, TX.

[14]Krishnamurthy, K., Barmore, B., Bussink, F., Weitz, L., and Dahlene, L., "Fast-Time Evaluations of Airborne Merging and Spacing in Terminal Area operations," AIAA Guidance, Navigation, and Control Conference and Exhibit 15 - 18 August 2005, San Francisco, California.

[15]Houston, V. E., and Barmore, B., "An Exploratory Study of Runway Arrival Procedures: Time-Based Arrival and Self-Spacing," 9th AIAA Aviation Technology, Integration, and Operations Conference (ATIO) 21 - 23 September 2009, Hilton Head, South Carolina.

[16]Barmore, B. E., Abbot, T. E., Capron, W. R., and Baxley, B. T., "Simulation Results for Airborne Precision Spacing along Continuous Descent Arrivals," The 26th Congress of International Council of the Aeronautical Sciences (ICAS), 14 - 19 September 2008, Anchorage, Alaska.

[17]Abbott, T. S., "Speed Control Law for Precision Terminal Area In-Trail Spacing," NASA/TM-2002-211742, July, 2002.

[18]Levitt. I., and Weitz, L., "Towards Definging Required Interval Management Performance," Ninth USA/Europe Air Traffic Management Research and Development Seminar (ATM 2011), June 14-17, Berlin Germany.

[19]Verma, S., Lozito, S., and Trot, G., "Preliminary guidelines on Flight Deck Procedures for Very Closely Spaced Parallel Runway Operations", *Proceedings of the 26th International Congress on Aeronautical Sciences*, Sep 2008, Anchorage, Alaska.

[20]Balakrishnan, H., and Balachandran, C., "Efficient and Equitable Departure Scheduling in Real-Time: New Approaches to Old Problems", *USA/Europe Air Traffic Management R&D Seminar*, Barcelona, Spain, June 2007.

[21]Gupta, G., Malik, W., and Jung, Y. C., "Incorporating Active Runway Crossing in Airport Departure Scheduling", *Proceedings of the AIAA Guidance, Navigation, and Control Conference*, Sep 2010, Toronto, Canada.

[22]Rathinam, S., Montoya, J., and Jung, Y. C., "An Optimization Model for Reducing Aircraft Taxi Times at the Dallas Fort Worth International Airport", *Proceedings of the 26th International Congress on Aeronautical Sciences*, Sep 2008, Anchorage, Alaska.

[23]Bott, T., Eisenhawer, S., Foggia, J., Brown, S., Lohr, G., Oseguera-Lohr, R., and Williams, D., "Performance Measures for a Runway Configuration Management Decision Support Tool", Presentation made at the NASA Airspace Systems Program Technical Interchange Meeting, Oct 2009, San Antonio, TX.

[24]Rapid Update Cycle (RUC): http://ruc.noaa.gov/, accessed on 07/22/2013

[25]Rapid Refresh (RAP): http://rapidrefresh.noaa.gov/ , accessed on 2/27/2013.

[26]MADIS website: http://madis.noaa.gov/, accessed on 2/27/2013.

[27]Aircraft Communications Addressing and Reporting System (ACARS) http://www.arinc.com/products/voice_data_comm/acars.html, accessed on 2/27/2013.

[28]Arnoldi Iteration: http://en.wikipedia.org/wiki/Arnoldi_iteration, accessed on 07/22/2013.

[29]Ren L., Clarke J-P. B., "Modeling and Simulating Wind Variation between Flights for Continuous Descent Arrival Implementation," *AIAA Modeling and Simulation Technologies Conference and Exhibit*, Honolulu, Hawaii, 18 - 21 August 2008.

[30]Cole R. E., Richard C., Kim S., and Bailey D., "An Assessment of the 60 km Rapid Update Cycle (RUC) with Near Real-Time Aircraft Reports," *Prepared for NASA Ames by Lincoln Laboratory MIT*, July 15, 1998.